Science Bulletin 62 (2017) 852–856

Contents lists available at ScienceDirect

Science Bulletin

journal homepage: www.elsevier.com/locate/scib

Article

Experimental signature of topological superconductivity and Majorana zero modes on β-Bi_2Pd thin films

Yan-Feng Lv [a], Wen-Lin Wang [a], Yi-Min Zhang [a], Hao Ding [a], Wei Li [a,b], Lili Wang [a,b], Ke He [a,b], Can-Li Song [a,b,*], Xu-Cun Ma [a,b], Qi-Kun Xue [a,b,*]

[a] State Key Laboratory of Low-Dimensional Quantum Physics, Department of Physics, Tsinghua University, Beijing 100084, China
[b] Collaborative Innovation Center of Quantum Matter, Beijing 100084, China

ARTICLE INFO

Article history:
Received 2 May 2017
Received in revised form 8 May 2017
Accepted 8 May 2017
Available online 11 May 2017

Keywords:
Epitaxial β-Bi_2Pd films
Molecular beam epitaxy
Topological superconductivity
Majorana zero modes
Scanning tunneling microscopy

ABSTRACT

The search for Majorana fermions in topological superconductors is one of paramount research targets in physics today. Using a cryogenic scanning tunneling microscopy, we here report the signature of topologically nontrivial superconductivity on a single material of β-Bi_2Pd films grown by molecular beam epitaxy. The superconducting gap associated with spinless odd-parity pairing opens on the surface and appears much larger than the bulk one due to the Dirac-fermion enhanced parity mixing of surface pair potential. Zero bias conductance peaks, probably from Majorana zero modes supported by such superconducting states, are identified at magnetic vortices. The superconductivity exhibits resistance to nonmagnetic defects, characteristic of time-reversal-invariant topological superconductors. Our study reveals β-Bi_2Pd as a prime platform to generate, manipulate and braid Majorana zero modes for quantum computation.

1. Introduction

Topological superconductors (TSCs) are a novel quantum phase of matter characterized by a fully gapped bulk state and gapless boundary states hosting exotic Majorana fermions that are their own anti-particles [1]. The Majorana fermions obey non-Abelian braiding statistics and could be useful for fault-tolerant quantum computers [2,3]. Following theoretical proposals [4–8], several experiments have disclosed their signatures in semiconductor nanowires [9,10], iron atomic chains [11] and topological insulators [12,13] by proximity to classical superconductors, all sharing complex hybrid heterostructures. Alternatively, the newly discovered single-component superconductors, such as Cu/Sr/Nb-doped Bi_2Se_3 [14–16], Weyl semi-metal TaAs single crystal [17], In-doped SnTe [18] and $PbTaSe_2$ [19], have been suggested as potential TSC candidates, but far from a final conclusion [20].

Tetragonal Bi_2Pd (hereafter, β-Bi_2Pd) crystallizes into a simple $CuZr_2$-type (I4/mmm) structure (Fig. 1a), and exhibits classical *s*-wave bulk superconductivity with a transition temperature (T_c) close to 5.4 K [21]. Intriguingly, it was recently demonstrated from angle-resolved photoemission spectroscopy (ARPES) that β-Bi_2Pd holds several topologically protected surface bands cross the Fermi level (E_F) [22]. The nontrivial surface states of β-Bi_2Pd are subject to a classical *s*-wave bulk pairing, which naturally satisfies the key ingredients of proximity-induced two-dimensional (2D) topological superconductivity near the surface [4]. Here the proximity induced electron pairing on the spin-momentum-locked topological surface has a nontrivial topology and is obliged to be effectively spinless *p*-wave so as to guarantee the pair wave function antisymmetric [4,23,24]. Such superconducting states are anticipated to carry Majorana zero modes (MZMs) at the end of magnetic vortex lines, and thus reignite numerous research interests in β-Bi_2Pd. However, the subsequent studies consistently reveal a conventional *s*-wave superconductivity [25–27] and no MZM at vortices of β-Bi_2Pd single crystals [28]. In this work, we used a state-of-the-art molecular beam epitaxy (MBE) in ultrahigh vacuum (UHV) to prepare β-Bi_2Pd thin films on $SrTiO_3$(001) substrate and characterized their superconductivity with *in situ* scanning tunneling microscope (STM). We found the experimental evidence for nontrivial and impurity-resistant superconducting gap opening on the surface, as well as possible MZMs at vortices.

2. Experimental

Our experiments were conducted in a cryogenic STM apparatus, connected with a MBE chamber for sample preparation. The base

* Corresponding authors.
E-mail addresses: clsong07@mail.tsinghua.edu.cn (C.-L. Song), qkxue@mail.tsinghua.edu.cn (Q.-K. Xue).

http://dx.doi.org/10.1016/j.scib.2017.05.008
2095-9273/

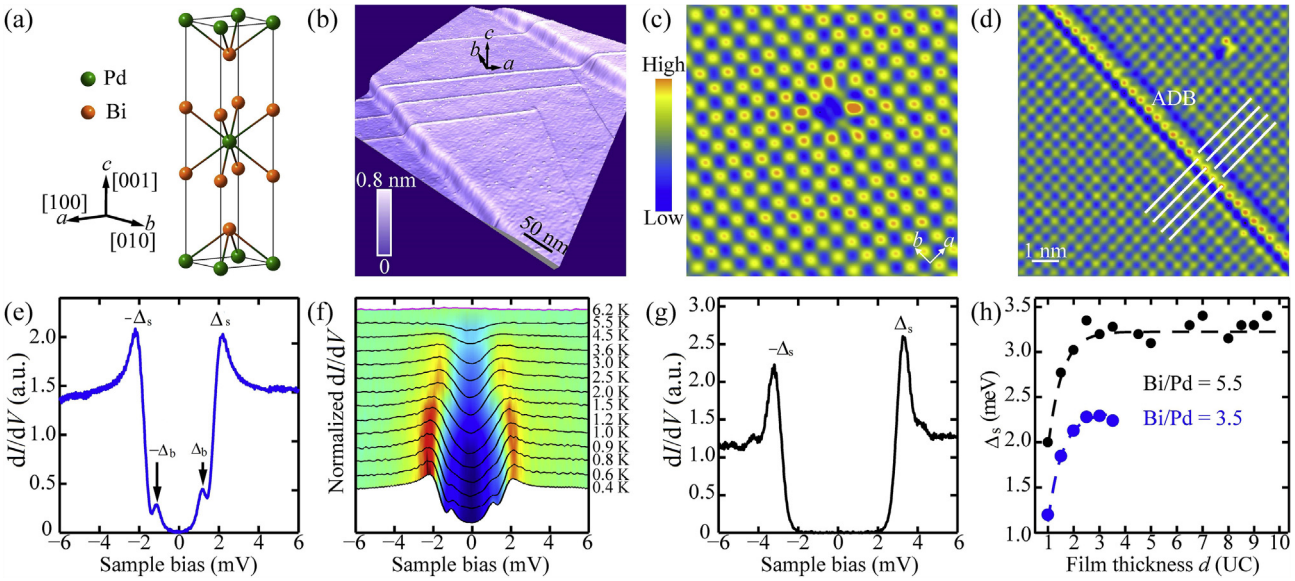

Fig. 1. (Color online) STM characterization of topologically superconducting β-Bi_2Pd films on $SrTiO_3$. (a) Crystal structure of β-Bi_2Pd. Each Pd atom sits at the center of the square prism of eight Bi atoms and the resulting Bi_2Pd motifs are stacked alternately by weak van der Waals forces, forming a body-centered layered structure. The *a*, *b* and *c* axes are taken along the crystal orientations. Along the *c*(001) direction, each unit cell consists of two Bi-Pd-Bi triple layers. (b) STM topography (V = 4.0 V, I = 30 pA, 400 nm × 400 nm) of ~20 UC thick β-Bi_2Pd films, grown with a Bi/Pd flux ratio of 3.1. The bright spots and linear protrusions correspond to Bi adatoms and ADB defects, respectively. The ADBs are orientated along either of the two in-plane crystallographic axes. Unless otherwise specified, our measurements are performed on this films. (c) Zoom-in image of β-Bi_2Pd surface (V = 2 mV, I = 280 pA, 4.5 nm × 4.5 nm), displaying a single Bi vacancy. The bright spheres indicate Bi atoms in the top layer. (d) A magnified ADB (V = −1 mV, I = 300 pA, 8 nm × 8 nm). The eight white lines show a lattice shift in the *b*–*c* atomic planes across the ADB by half of the lattice parameter along the *a* axis (1.7 Å). (e) Differential conductance d*I*/d*V* spectrum on the thick β-Bi_2Pd films grown with a Bi/Pd flux ratio of 5.5 (b) at 0.4 K, revealing two distinct superconducting gaps, denoted as Δ_s and Δ_b, respectively. Spectra are acquired with a sample bias voltage of V = 10 mV and tunneling current of I = 300 pA throughout. (f) Temperature dependence of d*I*/d*V* spectra in β-Bi_2Pd, displaying completely vanishing gap at 6.2 K (magenta curve). (g) d*I*/d*V* spectrum on β-Bi_2Pd films prepared with a larger Bi/Pd flux ratio of 5.5. (h) Pairing gap Δ_s versus both the film thickness *d* and Bi/Pd flux ratio. Dashed lines are guide to the eye.

pressure of both systems is better than 1.0×10^{-10} Torr (1 Torr ≈ 133.322 Pa). Nb-doped (0.05 wt%) $SrTiO_3$(001) substrates were outgassed in UHV and then annealed at 1200 °C to obtain clean surface. The β-Bi_2Pd films were prepared by co-evaporating high-purity Pd (99.99%) and Bi (99.999%) sources from standard Knudsen cells under Bi-rich condition, with the substrate held at 300–350 °C. More details are discussed in the Electronic Supplementary Material (online). Polycrystalline PtIr tip was cleaned in UHV and calibrated on MBE-grown Ag films prior to all STM measurements at 0.4 K, unless otherwise specified. The differential conductance d*I*/d*V* spectra and maps were collected using a standard lock-in technique with a small bias modulation of 0.1 mV at 913 Hz.

3. Results and discussion

MBE growth of β-Bi_2Pd films on $SrTiO_3$ substrate proceeds in Volmer-Weber mode. Epitaxial islands down to a single unit-cell (UC, two Bi-Pd-Bi triple layers) thick with lateral size of several hundreds of nanometers could be prepared, as seen from Fig. S1 (online). We have also established the growth dynamics of high-quality β-Bi_2Pd crystalline films by MBE, as detailed in the Electronic Supplementary Material (online). Fig. 1b shows a constant-current STM topographic image on the atomically flat Bi-terminated (001) β-Bi_2Pd films, grown by using a Bi/Pd flux ratio of 3.1. The films are found to straddle continuously over the neighboring terraces, indicative of a "carpetlike" growth of β-Bi_2Pd across the underlying $SrTiO_3$ steps. The adjacent Bi atoms are spaced ~3.4 Å apart (Fig. 1c), while the out-of-plane lattice constant is approximate to 1.3 nm (Fig. S1 online). They match excellently with those in β-Bi_2Pd crystals [21] and β-Bi_2Pd thin films prepared on Bi/Si(111) substrate [29], justifying the chemical identity of epitaxial films studied here as β-Bi_2Pd. Because other Pd-Bi intermediate compounds all exhibit sharply different crystal structures and lattice parameters from our experimental observations [30]. Furthermore, the similar electron band structure between the MBE-grown thin films and β-Bi_2Pd crystals, revealed by ARPES [21,29], unambiguously backups this claim. Finally, we found no other spurious phase in all samples investigated and the lattice constants alter little with film thickness *d*. This indicates a negligibly small strain involved, as expected for quasi van der Waals epitaxy of layered β-Bi_2Pd on $SrTiO_3$. Two distinct kinds of surface defects, namely Bi vacancy (Fig. 1c) and Bi adatom (Fig. 1b), as well as anti-phase domain boundary (ADB) (Fig. 1d) are identified.

Scanning tunneling spectroscopy (STS) probes the local density of states (DOS) and can measure the superconducting gap at E_F. In order to minimize the possible strain effects, we measured the tunneling conductance d*I*/d*V* spectrum on a thick (~26 nm) β-Bi_2Pd films. Fig. 1e depicts a typical d*I*/d*V* spectrum at the base temperature of 0.4 K. In sharp contrast to single-gap superconductivity reported for bulk counterpart [25–28], two pairs of conductance peaks at two different energy scales are noticed, indicating double superconducting gaps in the β-Bi_2Pd films. The smaller one with a low spectral weight is estimated to be (1.0 ± 0.1) meV, close to the reported values of 0.76–0.92 meV in bulk β-Bi_2Pd [25–28]. This hints at its possible origin from the bulk states and we thus dub it as Δ_b for simplicity. On the other hand, the newly discovered gap, which we reveal below stems from the topological surface states of β-Bi_2Pd and is dubbed as Δ_s, is more prominent and significantly enhanced in magnitude.

The temperature-dependent d*I*/d*V* spectra have been performed to decipher the origin of Δ_s in the epitaxial β-Bi_2Pd films, as plotted in Fig. 1f. At elevated temperatures, the Δ_s is gradually smeared out and vanishes below 6.2 K. This result is surprising: the larger Δ_s of 2.15 meV would have led to a much higher T_c (13 K or higher assuming the reduced gap ratio $2\Delta/k_BT_c = 3.7–4.1$ for β-Bi_2Pd [25–28]) if it stems from another bulk band in β-Bi_2Pd [21]. The

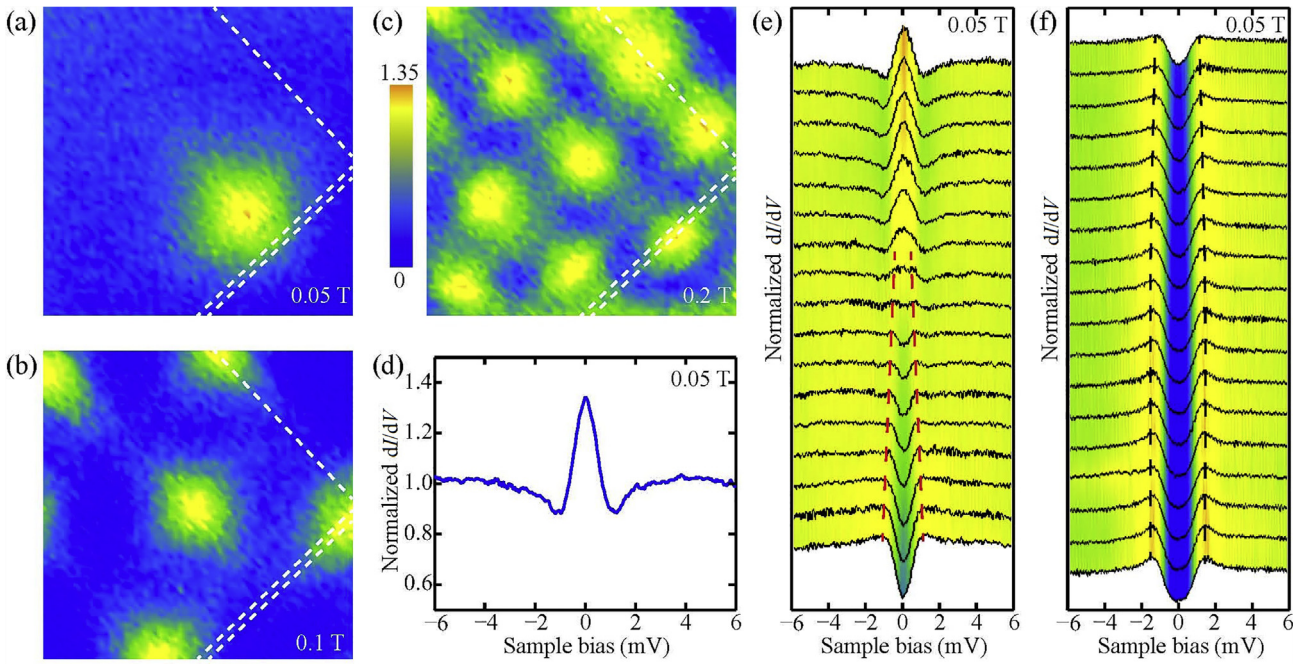

Fig. 2. (Color online) Magnetic vortices and ZBCPs at vortex cores. (a)–(c) Normalized zero-bias conductance maps (setpoint: V = 10 mV and I = 200 pA, 350 nm × 350 nm) at varying magnetic fields, showing individual vortices. The normalization was performed by dividing all raw ZBC maps by the conductance value at a high sample bias of 6 meV. (d) Tunneling conductance dI/dV spectrum taken at the vortex center, signifying the appearance of salient ZBCP. (e), (f) Normalized dI/dV spectra measured at locations with varying radial distance r from the vortex center. Here r alters from 0 (up) to 40 nm (down) with an equal separation of 2.5 nm in (e), and from 42 nm (up) to 144 nm (down) with an equal separation of 6 nm in (f), respectively. The ZBCPs are localized on a length scale of about 12 nm and show no splitting away from the vortex center. The dashed lines mark the evolution of Δ_s.

other possibility is that Δ_s might has a root at the surface of epitaxial β-Bi_2Pd thin films, given the existence of topological surface states on β-Bi_2Pd [22]. In general, parity mixing of pair potential would occur near the surface of a superconductor due to the broken inversion symmetry there. Theoretically, the presence of Dirac fermions on the surface of β-Bi_2Pd might anomalously enhance such mixing of Δ_b and time-reversal-symmetry (TRS) protected odd-parity pairing, leading to a larger pair potential Δ_s near the surface [24]. This appears a virtual match with our finding.

Note that the absence of Δ_s in β-Bi_2Pd single crystals [28], as distinct from the epitaxial thin films, might be likely caused by a different E_F, where the surface states have merged into and are indistinguishable from the continuum bulk bands [23,24]. Theoretically, tuning the chemical potential to isolate the topological surface states from bulk bands near E_F can bring about nontrivial electron pairing at the surface, as probably already realized here. A careful comparison of the electron states around Γ does reveal an upward shift of E_F (~70 meV) in β-Bi_2Pd/Bi/Si(111) thin films [29] with respect to their bulk counterpart [21], although it is subject to a direct ARPES study of the β-Bi_2Pd films on $SrTiO_3$. Further defect engineering of E_F by growing β-Bi_2Pd with a higher Bi/Pd flux ratio of 5.5, which may further increase the separation between the bulk and surface bands, leads to a larger Δ_s of 3.3 meV (Fig. 1g). The enhanced surface gap Δ_s submerges Δ_b and has vanishing DOS over a finite energy range near E_F, as clearly seen in Fig. 1g. This indicates a nodeless pairing gap function for Δ_s, despite a slight anisotropy (Fig. S2 online). Finally, we find that Δ_s relies on the film thickness d and reduces abruptly below $d \sim 2.5$ UC (Fig. 1h). This is probably resulted from the suppressed bulk superconductivity of β-Bi_2Pd when approaching the 2D limit. Since Δ_s links closely with Δ_b [24], the reduced Δ_b will lead to a shrinking Δ_s. The gradual saturation of Δ_s on thick films ($d \geq 3$) echoes the above claim that the epitaxial stain is negligibly small in the β-Bi_2Pd films. As thus, we have compellingly revealed TSC near the surface of epitaxial β-Bi_2Pd films.

In order to shed further light on Δ_b, we have explored its dependence on magnetic field. Fig. 2a–c shows the zero bias conductance (ZBC) maps in varying magnetic field, which was applied perpendicular to the sample surface. The yellow regions with enhanced ZBC due to the suppressed superconductivity signify individual isolated vortices, exhibiting a slight four-fold symmetry. This could be understood by a difference between coherence length ξ along the crystal axes (a or b) and the diagonals, and matches with the observed gap anisotropy of Δ_s in Fig. S2 (online) since $\xi \sim 1/\Delta$. Below the critical field H_{c2}, the vortex increases linearly in number with the field, as expected. More remarkably, each vortex core presents the dI/dV spectrum with a salient ZBC peak (ZBCP) (Fig. 2d), which we will discuss later. Fig. 2e and f depicts the spatial dependence of dI/dV spectra in the vicinity of single magnetic vortex. We notice that in stark contrast to usual superconductors the surface gap Δ_s does not recover to its zero-field value of 2.15 meV at position even larger than 100 nm from the vortex center (Fig. 2f). This further supports the topologically nontrivial nature of Δ_s, which we explain below.

Specifically, in common type-II superconductors the superconducting order parameter Δ regains its zero-field value outside the vortex core within the coherence length ξ, ~23 nm in β-Bi_2Pd [25], while the magnetic field H decays within a longer length scale (London penetration depth, λ). However, in TSCs, the magnetization around one vortex breaks the TRS and independently opens another insulating gap in the surface Dirac spectrum [4,31]. This gap competes with and effectively weakens the superconducting gap Δ. One thus anticipates that the superconductivity outside the vortex core of TSCs recovers in a longer length scale of λ (>100 nm) other than ξ [25]. Our finding coincides with this expectation in a prominent manner. As summarized in Fig. 3a, the

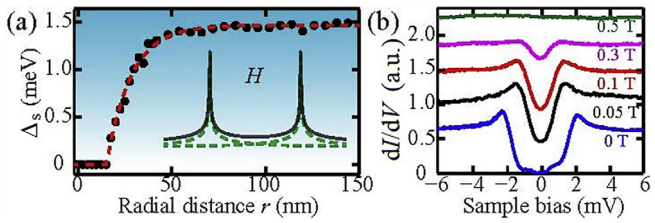

Fig. 3. (Color online) Magnetic field effect on Δ_s. (a) Gap magnitude of Δ_s plotted as a function of radial distance r from the vortex center at 0.05 T. Note that Δ_s does not recover its zero-field value of 2.15 meV even far from the vortex center. Inset shows how the fields from isolated vortices (green dashes) overlap. Gray line corresponds to the overlapping field H. (b) Field-dependent dI/dV spectra in-between adjacent vortices, revealing a reduced gap Δ_s at elevated field. The zero-field spectrum (blue curve) is redrawn for comparison.

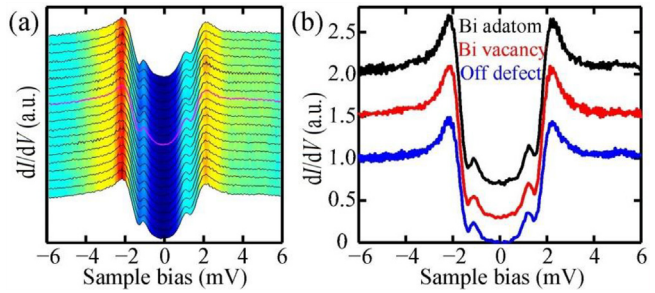

Fig. 4. (Color online) TRS protected topological pairing gap Δ_s. (a) A series of dI/dV spectra crossing an ADB, equally spaced 0.5 nm apart along a 10-nm trajectory. The magenta curve marks the spectrum on the ADB. (b) Comparison of superconducting energy gaps on and off Bi defects.

surface gap Δ_s increases with the radial distance r and seemingly saturates at 1.45 meV (still smaller than 2.15 meV) when r exceeds three times of ξ (~70 nm). Here the saturation behavior of Δ_s might be caused by the overlap of field H from the circulating supercurrents of adjacent vortices, as schematically inserted in Fig. 3a. At 0.05 T, the adjacent vortices are spaced only 219 nm. The fields around individual isolated vortices (green dashes) overlap, which consequently produces a very slowly varying H in between (gray line). This leads to a negligibly small change of Δ_s with r which is difficult to be resolved, when r is moderately large. A further increase of the applied field enhances the overlapping field H and consequently reduce Δ_s in between adjacent vortices. As shown in Fig. 3b, our experiment indeed confirms this conjecture. It is worthy to note that this observation contrasts sharply from the behavior of trivial bulk gap Δ_b under magnetic fields, where the field H fills the in-gap DOS but little changes the gap magnitude [28]. This observation further solidifies the topologically nontrivial nature of Δ_s.

In distinction to the chiral p-wave superconductor, the effectively spinless superconductivity Δ_s realized here respects TRS and are topologically protected against scattering by TRS invariant nonmagnetic impurity [4], as the conventional s-wave superconductor does [32]. Fig. 4a and b plots the dI/dV spectra cross an ADB and on intrinsic Bi defects, respectively. No variation of Δ_s is observed as the STM tip is atop the ADB (Fig. 4a), Bi adatom and Bi vacancy (Fig. 4b). This is consistent with the topological nature of Δ_s protected by TRS.

Finally, we comment on the nature of ZBCPs identified at vortices (Fig. 2d). Distinct from bulk β-Bi_2Pd crystals [28], the ZBCPs observed here might originate from the ordinary Caroli-de Gennes-Matricon (CdGM) vortex bound states [33] or MZMs [4]. Since the topologically nontrivial superconducting states revealed above is expected to harbor MZMs at vortices [4], it is fairly straightforward to ascribe the ZBCPs to MZMs. This is further supported by studying the spatial dependence of dI/dV spectra in the vicinity of single magnetic vortex (Fig. 2e, f). The ZBCP shows no splitting when moving away from the vortex center and is invariably fixed to the zero energy until the pairing gap Δ_s (marked by the dashed lines) begins to develop at a radial distance $r \sim 14$ nm off the vortex core (Fig. 2e). This differs markedly from the superconducting $Bi_2Te_3/NbSe_2$ heterostructure, where the MZMs entangle with usual CdGM bound states and result into a sophisticated space-dependent splitting of ZBCPs around the vortices [12,13]. The identity of ZBCP observed as possible MZM (or at least contains the component of MZMs), rather than trivial CdGM bound state, receives further evidence from the vanishing peak-dip structure outside Δ_s induced by the scattering states (Fig. 2d, e), which are often accompanied with trivial CdGM states bounded at vortices [34]. Nevertheless, further investigation is desirable to fully understand the nature of ZBCPs observed here.

4. Summary

Our observation of TSC in one material of β-Bi_2Pd films has pointed to a novel avenue for searching topological pairing states on ordinary superconductors that possess topologically nontrivial surface states by E_F engineering. This way dispels the structural complexity and interface unpredictability in artificial hybrid TSCs [9–13] and can mostly avoid the interruption from other non-topological alternatives (e.g. Kondo effect, disorder or impurity scattering) on MZMs [35–37]. As for β-Bi_2Pd, further growth control and electronic structure characterization are desired to finely tune its chemical potential and study the crossover from a topologically trivial superconductivity to the nontrivial one as reported here. Finally, analogous to the hybrid TSCs [11–13], the possible MZMs (Fig. 2d) are found to manifest a large peak width of ~0.8 meV beyond the thermal broadening, probably caused by their coupling to vortex-induced subgap states [38]. An important next step in clarifying this issue would be to explore how such fermionic states affects the MZM broadening.

Conflict of interest

The authors declare that they have no conflict of interest.

Acknowledgments

The work was financially supported by the National Natural Science Foundation of China, Ministry of Science and Technology and Ministry of Education of China. C. L. S. acknowledges supports from the National Thousand-Young-Talents Program and the Tsinghua University Initiative Scientific Research Program.

Appendix A. Supplementary data

Supplementary data associated with this article can be found, in the online version, at http://dx.doi.org/10.1016/j.scib.2017.05.008.

References

[1] Majorana E. Symmetrical theory of electrons and positrons. Nuovo Cimento 1937;14:171–84.
[2] Kitaev AY. Unpaired Majorana fermions in quantum wires. Phys Usp 2001;44:131–6.
[3] Elliott SR, Franz M. Colloquium: Majorana fermions in nuclear, particle, and solid-state physics. Rev Mod Phys 2015;87:137–63.
[4] Fu L, Kane CL. Superconducting proximity effect and Majorana fermions at the surface of a topological insulator. Phys Rev Lett 2008;100:096407.
[5] Qi XL, Hughes TL, Raghu S, et al. Time-reversal-invariant topological superconductors and superfluids in two and three dimensions. Phys Rev Lett 2009;102:187001.

[6] Sau JD, Lutchyn RM, Tewari S, et al. Generic new platform for topological quantum computation using semiconductor heterostructures. Phys Rev Lett 2010;104:040502.
[7] Oreg Y, Refael G, von Oppen F. Helical liquids and Majorana bound states in quantum wires. Phys Rev Lett 2010;105:177002.
[8] Choy TP, Edge JM, Akhmerov AR, et al. Majorana fermions emerging from magnetic nanoparticles on a superconductor without spin-orbit coupling. Phys Rev B 2011;84:195442.
[9] Mourik V, Zuo K, Frolov SM, et al. Signatures of Majorana fermions in hybrid superconductor-semiconductor nanowire devices. Science 2012;336:1003–7.
[10] Albrecht SM, Higginbotham AP, Madsen M, et al. Exponential protection of zero modes in Majorana islands. Nature 2016;531:206–9.
[11] Nadj-Perge S, Drozdov IK, Li J, et al. Observation of Majorana fermions in ferromagnetic atomic chains on a superconductor. Science 2014;346:602–7.
[12] Xu JP, Wang MX, Liu ZL, et al. Experimental detection of a Majorana mode in the core of a magnetic vortex inside a topological insulator-superconductor $Bi_2Te_3/NbSe_2$ heterostructure. Phys Rev Lett 2015;114:017001.
[13] Sun HH, Zhang KW, Hu LH, et al. Majorana zero mode detected with spin selective Andreev reflection in the vortex of a topological superconductor. Phys Rev Lett 2016;116:257003.
[14] Fu L, Berg E. Odd-parity topological superconductors: theory and application to $Cu_xBi_2Se_3$. Phys Rev Lett 2010;105:097001.
[15] Sasaki S, Kriener M, Segawa K, et al. Topological superconductivity in $Cu_xBi_2Se_3$. Phys Rev Lett 2011;107:217001.
[16] Liu ZH, Yao X, Shao JF, et al. Superconductivity with topological surface state in $Sr_xBi_2Se_3$. J Am Chem Soc 2015;137:10512.
[17] Wang H, Wang HC, Chen YQ, et al. Discovery of tip induced unconventional superconductivity on Weyl semimetal. Sci Bull 2017;62:425–30.
[18] Novak M, Sasaki S, Kriener M, et al. Unusual nature of fully gapped superconductivity in In-doped SnTe. Phys Rev B 2013;88:140502.
[19] Guan SY, Chen PJ, Chu MW, et al. Superconducting topological surface states in the noncentrosymmetric bulk superconductor $PbTaSe_2$. Sci Adv 2016;2:e1600894.
[20] Levy N, Zhang T, Ha J, et al. Experimental evidence for *s*-wave pairing symmetry in superconducting $Cu_xBi_2Se_3$ single crystals using a scanning tunneling microscope. Phys Rev Lett 2013;110:117001.
[21] Imai Y, Nabeshima F, Yoshinaka T, et al. Superconductivity at 5.4 K in β-Bi2Pd. J Phys Soc Jpn 2012;81:113708.
[22] Sakano M, Okawa K, Kanou M, et al. Topologically protected surface states in a centrosymmetric superconductor β-$PdBi_2$. Nat Commun 2015;6:8595.
[23] Hao L, Lee TK. Surface spectral function in the superconducting state of a topological insulator. Phys Rev B 2011;83:134516.
[24] Mizushima T, Yamakage A, Sato M, et al. Dirac-fermion-induced parity mixing in superconducting topological insulators. Phys Rev B 2014;90:184516.
[25] Kačmarčík J, Pribulová Z, Samuely T, et al. Single-gap superconductivity in β-Bi_2Pd. Phys Rev B 2016;93:144502.
[26] Biswas PK, Mazzone DG, Sibille R, et al. Fully gapped superconductivity in the topological superconductor β-$PdBi_2$. Phys Rev B 2016;93:220504.
[27] Che L, Le T, Xu CQ, et al. Absence of Andreev bound states in β-$PdBi_2$ probed by point-contact Andreev reflection spectroscopy. Phys Rev B 2016;94:024519.
[28] Herrera E, Guillam I, Galvis JA, et al. Magnetic field dependence of the density of states in the multiband superconductor β-Bi_2Pd. Phys Rev B 2015;92:054507.
[29] Denisov NV, Matetskiy AV, Tupkalo AV, et al. Growth of layered superconductor β-$PdBi_2$ films using molecular beam epitaxy. Appl Surf Sci 2017;401:142–5.
[30] Okamoto H. The Bi-Pd (Bismuth-Palladium) system. J Phase Equilib 1994;15:191–4.
[31] Burset P, Lu B, Tkachov G, et al. Superconducting proximity effect in three-dimensional topological insulators in the presence of a magnetic field. Phys Rev B 2015;92:205424.
[32] Anderson PW. Theory of dirty superconductors. J Phys Chem Solids 1959;11:26–30.
[33] Caroli C, De Gennes PG, Matricon J. Bound fermion states on a vortex line in a type-II superconductor. Phys Lett 1964;9:307–9.
[34] Gygi F, Schlüter M. Self-consistent electronic-structure of a vortex in a type-II superconductor. Phys Rev B 1991;43:7609–21.
[35] Liu J, Potter AC, Law KT, et al. Zero-bias peaks in the tunneling conductance of spin-orbit-coupled superconducting wires with and without Majorana end-states. Physical Review Letters 2012;109:267002.
[36] Sau JD, Brydon PMR. Bound states of a ferromagnetic wire in a superconductor. Physical Review Letters 2015;115:127003.
[37] Churchill HOH, Fatemi V, Grove-Rasmussen K, et al. Superconductor-nanowire devices from tunneling to the multichannel regime: zero-bias oscillations and magnetoconductance crossover. Phys Rev B 2013;87:241401.
[38] Das Sarma S, Nag A, Sau JD. How to infer non-Abelian statistics and topological visibility from tunneling conductance properties of realistic Majorana nanowires. Phys Rev B 2016;94:03514.